JCTC Journal of Chemical Theory and Computation

The Hydrated Electron as a Pseudo-Atom in Cavity-Bound Water Clusters

Alexis Taylor,[†] Chérif F. Matta,[†,‡] and Russell J. Boyd*[,†]

Department of Chemistry, Dalhousie University, Halifax, NS, Canada B3H 4J3, and Department of Chemistry and Physics, Mount Saint Vincent University, Halifax, NS, Canada B3M 2J6

Received November 9, 2006

Abstract: Anionic water clusters, $(H_2O)_n^-$, of various sizes, $n = 1-8$, have been investigated using high-level ab initio calculations and the quantum theory of atoms in molecules, which provides a topological analysis of the electron density. The results of the current study indicate that the distribution of the excess electron is dependent on the geometry of the cluster. Non-nuclear attractors (NNAs), with associated pseudo-atomic basins and populations, are observed only in the highly symmetric clusters in which several non-hydrogen-bonded (NHB) hydrogen atoms are oriented toward a central cavity. For the latter cases, the non-nuclear attractor can be considered a pseudo-atom, possessing a significant portion of the excess electron within the cavity, consistent with the cavity-bound model of the solvated electron. In some cases, the population of the NNA is more than 0.2 electrons, and it contributes in excess of 20 kJ/mol to the energy of the system. Furthermore, the less symmetric systems, which tend to orient the NHB hydrogen atoms away from the center of the cluster, tend to delocalize the excess electron to a greater extent over several atoms at the surface of the cluster, consistent with the surface-bound model of the excess electron.

I. Introduction

While the solvated electron in water has been the focus of many experimental and theoretical studies, the microscopic structure of this species remains the subject of intense theoretical and experimental interest.[1−31] Water is the universal solvent; it is ubiquitous throughout our natural environment, from biological systems to interstellar space. For instance, hydrated electrons (anionic water clusters) are known to react with O_2 to produce the superoxide anion, O_2^-.[32,33] This reaction can occur in various conditions, in clouds, where O_2^- can destroy ozone,[34] to biological systems, where O_2^- is involved in cell death, aging, and various disease processes.[35] Given that anionic water has such a profound influence on a large variety of systems, a thorough understanding of its properties and behavior is essential.

As early as 1810, Humphry Davy observed that, when alkali metals are exposed to ammonia, the resulting solution has an intense blue color. The following century saw a great deal of research that focused on this phenomenon and sought to determine the cause. Although it was well-established that these solutions behave as electrolytes, possessing high conductivity and magnetic susceptibility,[36] it was not until nearly 100 years after Davy's observations that Kraus suggested that the solutions contain sodium cations and free electrons,[37] and that the latter are responsible for the intense color.

The discovery of solvated electrons in ammonia solutions led naturally to the assumption that solvated electrons might be observed in water. Indeed, water's larger dipole moment and stronger hydrogen-bonding capability facilitate the ionization of metals. However, it was another 50 years before hydrated electrons were generated by pulse radiolysis and observed in water.[38−40] In addition, it was found that this species was highly reactive and could be destroyed through

* Corresponding author e-mail: Russell.Boyd@dal.ca.
[†] Dalhousie University.
[‡] Mount Saint Vincent University.

10.1021/ct600334w CCC: $37.00
Published on Web 03/24/2007

various processes. For example, free electrons are easily removed from solution by recombination with the protons produced from the autoionization of water. Thus, the hydrated electron exhibits a short, pH-dependent lifetime.[41]

Subsequent studies by Haberland and co-workers[27−30] established that the hydrated electron was not only produced in bulk solvent but also in clusters of a finite size, forming anionic water clusters, $(H_2O)_n^-$. Furthermore, water molecules in small clusters do not experience autoionization as tends to occur in bulk solvent, and thus the lifetime of the hydrated electron should be greater in these small clusters. This distinction proved advantageous for investigations into the nature of the hydrated electron, which has since been studied extensively both experimentally and theoretically (see Beyer et al.[12] and references therein).

Many methods are employed to generate solvated electrons: injection of energetic electrons into the solvent,[38−40] photoionization of water or a suitable precursor by ultraviolet radiation,[22,41−43] interaction of alkali metal surfaces with water,[44] supersonic expansion to generate neutral clusters followed by irradiation with a low-energy electron beam to generate the anions,[45,46] and laser vaporization.[12,47] Furthermore, several spectroscopic methods may be employed to detect the solvated electrons once they are generated, such as photoelectron and infrared spectroscopy and mass spectrometry. However, while there are many experimental methods available to produce hydrated electrons, and several techniques to detect them, the problem that remains is how to determine the exact structure, and consequently the nature, of the hydrated electron. Is the excess electron density largely localized to a region of space within the water clusters or is it smeared out and distributed over the electronegative oxygen atoms?

Two general models concerning the structure of the solvated electron have been proposed:[1,2,8,23,31,48−57] the surface-bound model (frequently referred to as the dipole-bound model) and the cavity-bound model. The cavity-bound model predicts the electron to be localized to a particular region in space within the center of the cluster, while the surface-bound model predicts the electron to be delocalized over several atoms on the surface of the cluster. Theoretical methods have been extensively employed to probe the electronic structure of anionic water clusters. Various ab initio and density functional theory (DFT) methods have been applied to smaller clusters[7,11,13−16,20,21,58−64] as well as molecular dynamic simulations of the bulk sovent.[24,26,48,65−67] It was suggested by Turi et al.[56] that the hydrated electron exists solely in the surface-bound state for clusters smaller than 45 water molecules, $(H_2O)_{45}^-$. However, this was recently contradicted in a study by Khan,[1] in which $(H_2O)_{14}^-$ exhibits both surface- and cavity-bound states depending on the geometry of the cluster. Futhermore, Khan also noted that the two states were nearly identical in energy. While the cavity model is experimentally supported by the appreciable volume increase upon the injection of electrons into the solvent,[68] it is still unclear as to which model provides a better description.

The quantum theory of atoms in molecules (QTAIM)[69−73] is based on the topological analysis of the electron density, $\rho(\mathbf{r})$, and is used to predict bonding interactions and atomic properties.[74] The electron density exhibits maxima at the locations of the nuclei (or, more generally, the attractors) and lines of maximum electron density linking bonded nuclei, that is, bond paths. The resulting network of nuclei and bond paths represents the molecular graph for a given system. A *single* bond path always links the nuclei of chemically bonded atoms regardless of the bond order.[74] The bond path is always accompanied by a virial path, a line of maximally stabilizing potential energy density linking the same bonded nuclei.[75] The presence of a bond path and its associated virial path provides a definitive criterion for bonding, especially in ambiguous or borderline cases.[76] A bond path between nuclei is always accompanied by an interatomic surface (IAS) between the bonded atoms, and this IAS must satisfy the zero-flux condition[69]

$$\nabla\rho(\mathbf{r})\cdot\mathbf{n}(\mathbf{r}) = 0 \qquad (1)$$

for all $\mathbf{r}$'s on the surface $S(\mathbf{r})$, where $\nabla\rho(\mathbf{r})$ is the gradient of the electron density and $\mathbf{n}(\mathbf{r})$ is a unit vector normal to the surface. This IAS partitions the system into atomic regions or basins. The atoms defined in this manner, based on the topology of the electron density, were brought into coincidence with the quantum mechanically derived atoms in a molecule[77] starting from Schwinger's principle of stationary action.[78] The atoms in a molecule were shown to behave as "proper open quantum systems"[77] which are described by equations of motion in correspondence to closed total systems.[79] The atoms in molecules, when defined as proper open systems, recover and predict a wide range of experimental observations.[80]

The zero-flux surface consists of a set of $\nabla\rho(\mathbf{r})$ trajectories that originate at infinity and terminate at a single point in the electron density where $\nabla\rho(\mathbf{r}) = 0$, known as the bond critical point (BCP). Two other trajectories originate at the BCP, and each of these terminates at one of the nuclei involved in the bonding, thereby defining the bond path. In addition to satisfying the zero-flux condition, all nonperiodic systems must satisfy the Poincaré−Hopf relationship

$$n - b + r - c = 1 \qquad (2)$$

where n stands for the number of attractors (e.g., nuclei), b for the number of bond paths, r for the number of rings, and c for the number of cages.[81]

An important feature of QTAIM is its ability to predict non-nuclear attractors (NNAs), which by definition are maxima in the electron density at a location other than that of the nuclei. The occurrence of NNAs is rare and was first theoretically predicted in alkali metal clusters[82−84] and later observed experimentally in metallic beryllium and magnesium.[85,86] NNAs behave as attractors in the basins of proper open systems bounded by a zero-flux surface and satisfy the above equation (eq 1), just as atomic nuclei behave topologically. For this reason, a NNA and its associated basin bounded by zero-flux surfaces are termed "pseudo-atoms" in a molecule, cluster, or crystal. Furthermore, for any system containing a NNA, the Poincaré−Hopf relationship (eq 2) must be modified to include both nuclei (or nuclear critical points, NCPs) and non-nuclear attractors (i.e., n = NCP + NNA).

QTAIM is used in this work to study the properties of the pseudo-atomic basin associated with the hydrated electron and to shed light on questions such as: is the excess electron localized to a specific region in space, or is it delocalized over the entire system? If the hydrated electron exists as a localized entity within the cluster, it will appear as a nonnuclear attractor. If, however, the excess electron is delocalized over the entire system, no NNA will be observed, and the excess charge will be distributed over several atoms in the system.

Besides its physical foundations, the advantage of real space partitioning of the electron population entailed by QTAIM over population analyses such as Mulliken population analysis (MPA) becomes particularly apparent when we consider the case of the solvated electron. QTAIM is able to predict NNAs and consequently determine the population of the associated pseudo-atomic basins. Therefore, should the excess electron exist as a localized entity in an interstitial space not associated with any atom in the cluster, QTAIM can determine exactly to what extent this occurs. Conversely, a MPA of the same system (or any other scheme which assigns atomic populations on the basis of contributions from atom-centered basis functions) would, by necessity, delocalize the excess electron and assign a zero population to any region in space lacking basis functions at its center. Hence, population analyses based on the contributions of basis functions to an atomic population cannot be used to study the solvated electron. The use of QTAIM in the analysis of the hydrated electron is a novel approach and, to our knowledge, has not been reported elsewhere.

II. Computational Details

All structures were optimized at the UMP2(full)/6−31++G-(2d,2p) level of theory and frequencies calculated at that level to ensure local minima have been located. Unpublished DFT results were also obtained at the B3LYP/6-31++G(2d,2p) level of theory and were found to give qualitatively similar results with minor differences in geometric parameters. The spin contamination was never in excess of 0.083% for any of the studied clusters. To validate our discussion of atomic energies, we obtained the energies and wavefunctions always at the same level of theory used for the geometry optimization. [To report atomic (and pseudo-atomic) energies, one cannot optimize the geometry with one basis set and obtain the wavefunction using a larger one as is commonly (and often justifiably) done to refine the electron density and several other atomic and molecular properties. This approach would invalidate the discussion of atomic and pseudo-atomic energies due to nonvanishing forces on the nuclei, each contributing an origin-dependent virial term. Thus, all wavefunctions in this work were obtained at the same level of theory used in the geometry optimization.]

All electronic structure calculations were performed using Gaussian 03.[87] Molecular graphs were obtained using AIM2000,[88] while the AIMPAC suite of programs,[89] implemented in the AIMALL97 software,[90] was used to analyze the electron densities and obtain atomic properties. The distribution of the excess electron was determined from the charge difference between the anionic cluster and the corresponding neutral cluster in the anionic geometry. The spin density isosurfaces, the spin density being the difference between the α- and β-spin densities, that is, $\rho^{spin}(\mathbf{r}) \equiv \rho^{\alpha}(\mathbf{r}) - \rho^{\beta}(\mathbf{r})$, were obtained using GaussView.[91] All reported spin density isosurfaces are the 0.001 au isosurface unless otherwise stated. Higher and lower densities were shown to give the same qualitative results.

Table 1. Relative Energies (kJ/mol) of the Anionic and Neutral Water Clusters

system		anion[a]	neutral
(H_2O)		0	−89.7
$(H_2O)_2$	**2A**	0	−58.2
	2B	+1.4	−58.2
$(H_2O)_4$	**4A**	0	−46.5
	4B	+13.2	−57.2
$(H_2O)_6$	**6A**	0	+7.4
	6B	−34.9	−57.5
$(H_2O)_8$	**8A**	0	−80.7
	8B	−12.5	−80.7

[a] The cavity-forming anionic clusters (A) were assigned a relative energy of zero for any given cluster size.

A note should be made about the color scheme employed in the figures. Various critical points appear in the molecular graphs and are colored as follows: BCPs are red dots, ring critical points (RCPs) are yellow dots, cage critical points (CCPs) are green dots, and NNAs are pink dots. The larger spheres represent the nuclei, employing the usual color scheme of oxygen as red spheres and hydrogen as white.

III. Results and Discussion

A. Water Anion, $(H_2O)^-$. The obvious starting point for any investigation into anionic water clusters is the monomer. Both anionic, $(H_2O)^-$, and neutral water were optimized at the UMP2(full)/6−31++G(2d,2p) level of theory, and the O−H bond lengths and the H−O−H bond angles were compared for the two cases. As may be expected, the addition of a single electron has little effect on the overall geometry, with an increase in the O−H bond of 0.013 Å and a decrease in the bond angle of 2.8°. However, while the structural changes are minor, the energetic changes are more significant; the anionic water molecule is 89.7 kJ/mol higher in energy than the neutral structure (see Table 1 for relative energies).

QTAIM was employed to determine the distribution of the excess electron, which was calculated from the difference between the atomic charges in the anionic structure and those in the corresponding neutral structure of the same geometry. The data indicate that a large portion of the excess electron is accommodated on the hydrogen atoms, 0.27 electrons (e^-) on each H atom with the remainder on the O atom, 0.44 e^- (Table 2). As one might expect, a greater proportion of the excess electron is accommodated on the oxygen atom when compared to a single hydrogen atom, due to its greater electronegativity. However, collectively, the hydrogen atoms accommodate a greater proportion of the excess electron. Analysis of the spin populations reveals a similar trend to that observed in the charge distribution, with a spin population of 0.42 on the oxygen atom and 0.29 on each hydrogen. The spin density plot graphically illustrates the distribution

Table 2. Selected Atomic Properties of the Anionic Water Clusters

cluster	atom	atomic charge (anion)	charge difference[a] (anion − neutral)	spin population	energy[b] (kJ/mol)
$(H_2O)^-$	O1	−1.6047	−0.4449	0.4197	
	H2	0.3072	−0.2727	0.2850	
	H3	0.3070	−0.2729	0.2852	
2A$^-$	O1	−1.3992	−0.2409	0.2036	
	H2	0.4537	−0.1255	0.1442	
	H3	0.4529	−0.1263	0.1448	
2B$^-$	O1	−1.2806	−0.0613	0.0369	
	H2	0.6491	+0.0237	0.0032	
	H3	0.5461	−0.0292	0.0216	
	O4	−1.5476	−0.3749	0.3526	
	H5	0.3223	−0.2736	0.2872	
	H6	0.3239	−0.2720	0.2859	
4A$^-$	O1	−1.3451	−0.1234	0.1020	
	H2	0.6443	−0.0018	0.0022	
	H3	0.4356	−0.1399	0.1609	
	NNA	**−0.0281**	**−0.0281**	**0.0277**	**−3.2**
4B$^-$	O1	−1.3423	−0.1094	0.1028	
	H2	0.6442	−0.0014	0.0037	
	H3	0.4596	−0.1380	0.1420	
6A$^-$	O1	−1.2853	−0.0733	0.0502	
	H2	0.6331	−0.0018	0.0025	
	H3	0.5281	−0.0486	0.0732	
	NNA	**−0.2318**	**−0.2318**	**0.2257**	**−21.5**
6B$^-$	H1	0.6345	−0.0025	0.0001	
	H2	0.6465	+0.0070	0.0002	
	H3	0.6347	−0.0038	0.0005	
	H4	0.6506	−0.0027	0.0002	
	O5	−1.2763	−0.0204	0.0053	
	O6	−1.2759	−0.0272	0.0048	
	O7	−1.2868	−0.0378	0.0145	
	O8	−1.2649	−0.0325	0.0148	
	H9	0.6274	+0.0134	0.0013	
	H10	0.6087	+0.0107	0.0014	
	H11	0.6274	+0.0249	0.0037	
	H12	0.5682	−0.0011	0.0229	
	H13	0.5471	−0.0443	0.0460	
	O14	−1.3159	−0.0821	0.0597	
	H15	0.6506	+0.0161	0.0046	
	O16	−1.4779	−0.3026	0.2830	
	H17	0.3294	−0.2756	0.2935	
	H18	0.3839	−0.2257	0.2362	
8A$^-$	O1	−1.2818	−0.0550	0.0372	
	H2	0.6496	−0.0005	0.0009	
	H3	0.5362	−0.0400	0.0589	
	NNA	**−0.2164**	**−0.2164**	**0.2101**	**−17.9**
8B$^-$	O1	−1.3647	−0.0980	0.1018	
	H2	0.6600	−0.0038	0.0021	
	H3	0.5105	−0.0900	0.0878	
	O4	−1.3253	−0.0553	0.0528	
	H5	0.6353	−0.0008	0.0031	
	H6	0.6348	−0.0021	0.0032	

[a] Charge difference was determined from the difference between the atomic charge in the anion and the atomic charge in the corresponding neutral cluster in the anionic geometry. [b] Only the total energies of the NNA basins (in kJ/mol) are reported here, since the energies of the other atoms are of too large to be reported in kJ/mol.

of the excess spin, which is predominantly located near the hydrogen atoms (Figure 1).

B. Anionic Water Dimers, $(H_2O)_2^-$. The optimization of the anionic monomer was followed naturally by an investigation of dimeric clusters. Two structures were investigated and optimized as seen in Figure 2, a cagelike structure in which the hydrogen atoms of the two water molecules are oriented toward one another, effectively forming a cavity between the two molecules (**2A**$^-$), and an approximately linear structure that exhibits the typical hydrogen-bonding arrangement (**2B**$^-$).

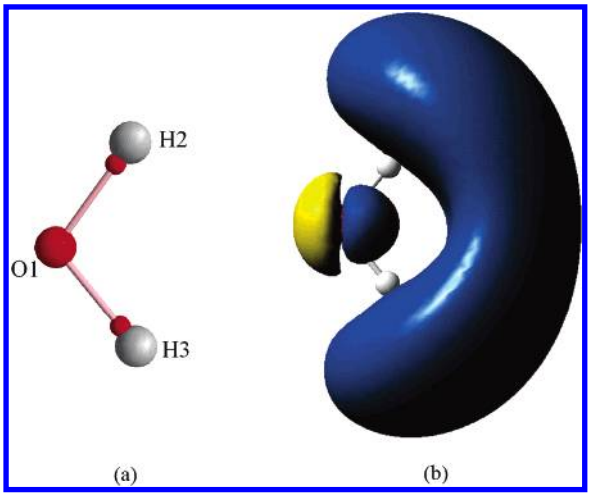

Figure 1. Molecular graph (a) of the water anion, $(H_2O)^-$, illustrating the bond critical points (BCP) between the nuclei and (b) the +0.001 and −0.001 au spin density isosurfaces (blue and yellow, respectively).

The molecular graph of **2A**$^-$ reveals that there is a long-range oxygen−oxygen interaction (∼5.2 Å) between the two water molecules as indicated by the BCP between the atoms. Once again, the H atoms accommodate a large portion of the excess electron, 0.13 e$^-$ each, while the O atoms possess a slightly larger fraction at 0.24 e$^-$, a trend that is mirrored in the spin populations of 0.14 and 0.20 for the hydrogen and oxygen atoms, respectively. The spin density plot of **2A**$^-$ (Figure 2) indicates that a large portion of the unpaired electron is found within the cavity formed by the two water molecules. Conversely, **2B**$^-$ tends to accommodate the excess electron preferably on the hydrogen-bond acceptor water molecule (0.27 e$^-$ on each H atom and 0.37 e$^-$ on the O atom from the integration data and spin populations of 0.29 and 0.35 for those same atoms; Table 2).

When the results of the two dimers are compared, it is obvious that there is a marked difference between the two systems. The highly symmetric **2A**$^-$ structure distributes the excess electron to a specific region within the center of the cluster, satisfying the notion of a cavity-bound hydrated electron. On the other hand, **2B**$^-$ delocalizes the electron over one of the water molecules, largely accommodating it on the surface of the cluster such that it may be considered surface-bound. However, it should also be noted, in either case (surface- or cavity-bound), the excess electron is largely accommodated by the NHB hydrogen atoms.

Additionally, structure **2A**$^-$ is marginally more stable than **2B**$^-$ by 1.4 kJ/mol. Although the energy difference is not very significant, it is interesting to note that the unusual cagelike arrangement has a stability similar to that of the typical water dimer upon the addition of an electron.

The geometries of each anionic dimer were subsequently used as initial structural coordinates for the optimization of a neutral cluster. Upon optimization, both structures prefer to adopt the typical hydrogen-bonding scheme, forming structure **2B** (Figure 2) which is very similar to **2B**$^-$ with some minor differences in geometric parameters [most notably a slightly longer hydrogen bond between the molecules and a smaller α angle (Figure 3)]. As may be

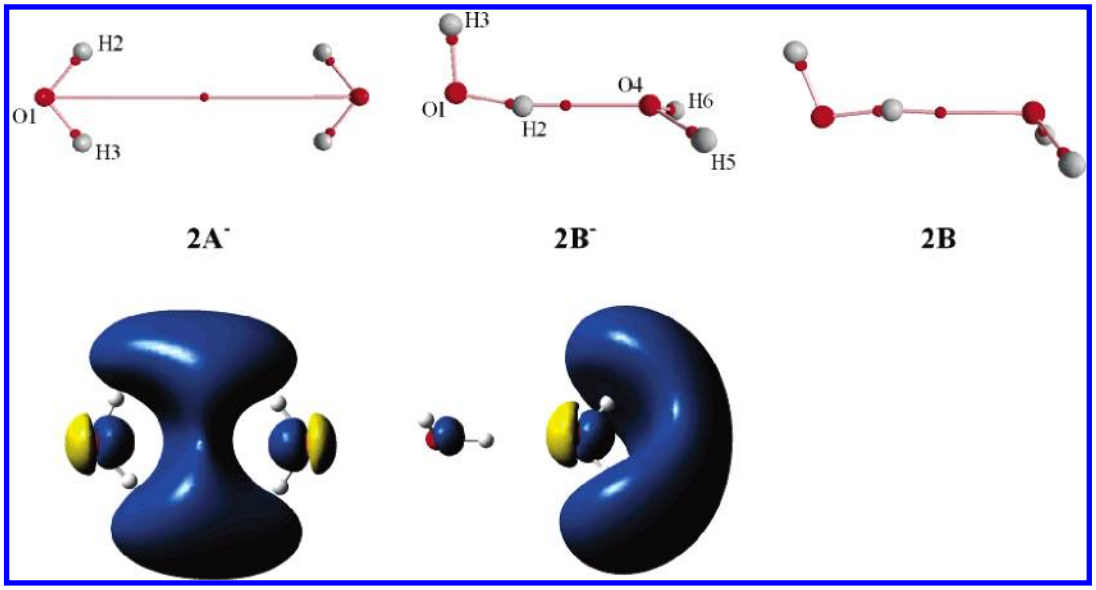

Figure 2. Molecular graphs of the optimized anionic dimer structures, **2A**$^-$ and **2B**$^-$, with their 0.001 au spin density plots shown below each structure as well as the optimized structure of the neutral water dimer, **2B**.

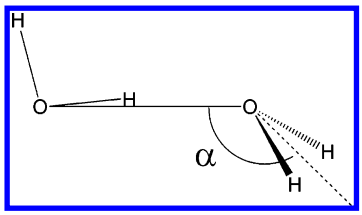

Figure 3. Neutral water dimer illustrating the α angle, the angle between the line connecting the oxygen atoms and the line bisecting the hydrogen atoms of the hydrogen-bond acceptor.

Table 3. Vertical Electron Dissociation Energies (VDE; eV) for the Anionic Water Clusters

system	VDE[a]	system	VDE[a]
monomer	0.918	**6A**	−0.476
2A	0.310	**6B**	−0.291
2B	0.573	**8A**	−0.613
4A	0.252	**8B**	0.696
4B	0.546		

[a] VDEs were calculated from the difference between the anion and the energy of the neutral cluster in the anion geometry.

expected, the neutral structure was the most stable of the three dimers investigated, almost 60 kJ/mol more stable than either of the anionic structures (Table 1).

Vertical electron dissociation energies (VDEs) were calculated from the energy difference between the anion and that of the corresponding neutral cluster in the anionic geometry. It was found that structure **2A**$^-$, the cavity-bound state, had a smaller VDE value, 0.310 eV, compared to that of **2B**$^-$, 0.573 eV, the surface-bound state (Table 3). This trend of smaller VDE values for the cavity-bound model compared to the surface-bound model is observed in all of the clusters studied and is in agreement with previous work in the field.[56]

It should be emphasized that other geometries are possible for the dimeric case previously discussed as well as the larger systems to be described below. First and foremost, the goal of the current study was to determine whether non-nuclear attractors exist topologically in anionic water clusters. Furthermore, for the systems in which NNAs are found, various characteristics of those systems were probed and compared to systems in which NNAs are absent. Therefore, the main focus was the comparison of two types of clusters for each cluster size investigated: those in which several NHB hydrogen atoms are contained within the cavity and those in which they protrude from the surface of the cluster. The current study is by no means an exhaustive search for all possible cluster geometries.

C. Anionic Water Tetramers, $(H_2O)_4^-$. Two tetrameric structures were investigated, both with four water molecules hydrogen-bonded in a single ring. **4A**$^-$ possesses a 4-fold axis of symmetry, with the NHB hydrogen atoms (or the out-of-plane H atoms) all pointed in the same direction, while in **4B**$^-$ the NHB hydrogen atoms alternate directions forming a cluster with a 2-fold axis of symmetry (Figure 4). Electronic structure optimizations reveal that **4A**$^-$ is more stable than **4B**$^-$ by 13.2 kJ/mol (Table 1), indicating that **4A**$^-$ is the energetically favored structure formed upon the addition of a single electron to the two systems investigated.

Although the two tetrameric structures share some similar features, a major difference becomes apparent from the QTAIM analysis: **4A**$^-$ possesses a NNA situated above the non-hydrogen-bonded H atoms, while **4B**$^-$ exhibits no such NNA. Because of this NNA in **4A**$^-$, five RCPs and one CCP are also observed (and are indeed necessary to satisfy the Poincaré−Hopf relationship), whereas **4B**$^-$ exhibits only one RCP (Figure 4). According to QTAIM, all maxima in the electron density are bounded by zero-flux surfaces, which separate each attractor from its neighbors. NNAs are no exception to this rule; they are bounded by zero-flux surfaces, which define a pseudo-atomic basin in which electron density resides. Indeed, the NNA can be considered to be a pseudo-atom, and QTAIM can be used to determine its electron population, which in the case of **4A**$^-$ is 0.03 e$^-$ (and a spin population of 0.03), as well as its contribution to the overall

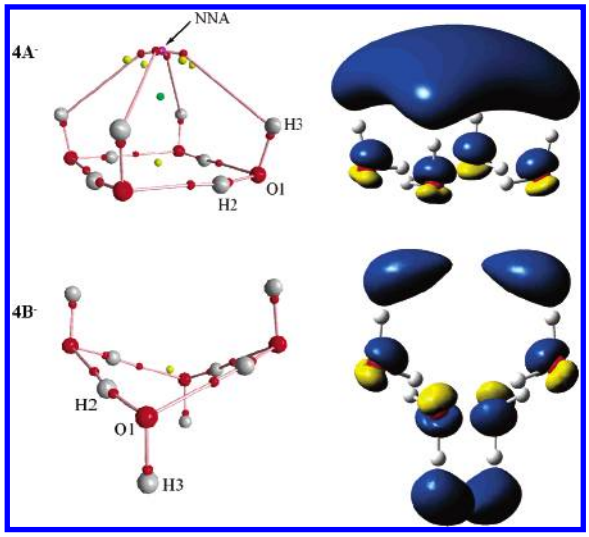

Figure 4. Molecular graphs of **4A**$^-$ and **4B**$^-$ as well as their 0.001 au spin density plots shown beside each structure. Note the appearance of the non-nuclear attractor (NNA) in the **4A**$^-$ system (pink sphere).

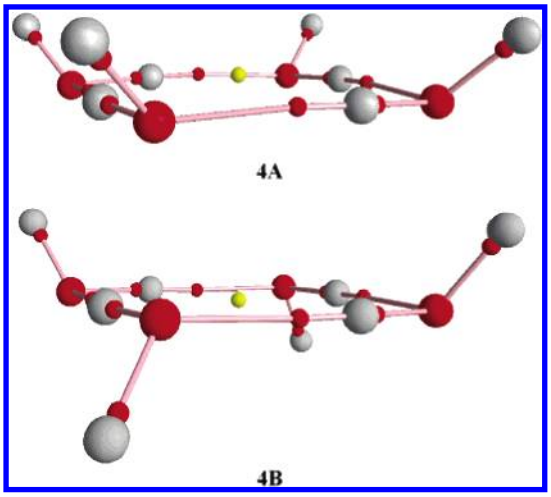

Figure 5. Optimized structures of the neutral water tetramers **4A** and **4B** (N.B., the neutral structures maintain a similar arrangement to the anionic clusters but flatten out considerably).

energy, 3.2 kJ/mol (Table 2), and a pseudo-atomic volume of 11.8 au. As a frame of reference for atomic volumes observed in these anionic clusters, we note that the hydrogen-bonded H atoms typically have volumes of 10 to 15 au; the NHB hydrogen atoms range from 30 to 90 au, and the oxygen atoms range from 140 to 200 au. Although the actual population and energy of the pseudo-atomic basin are small in this case, the fact that the NNA is predicted for this geometry is significant, indicating that it exists topologically within the electron density.

Furthermore, the spin density plots (Figure 4) can be used to illustrate the difference between the two systems, namely, that **4A**$^-$ localizes the excess electron to a specific region above the plane of the four water molecules (accommodating 0.14 e$^-$ and 0.12 e$^-$ on each NHB H atom and O atom, respectively, and 0.03 e$^-$ on the NNA with a similar trend in the spin populations; Table 2) while **4B**$^-$ distributes the electron over the NHB hydrogen atoms (0.14 e$^-$ each) and the O atoms (0.11 e$^-$ each), essentially binding the electron to the surface of the cluster.

The subsequent optimizations of the two systems as neutral clusters resulted in two new structures that retain the general features of the anions. The most notable change is the position of the NHB hydrogen atoms, which move away from the center of the rings, ultimately flattening the entire systems (Figure 5). Additionally, **4B** is no longer "V-shaped" like its anionic counterpart. The energy differences between the anion and neutral for **4A** and **4B** are −46.5 kJ/mol and −57.2 kJ/mol, respectively (see Table 1 for relative energies). While both of the neutral structures are more stable than their corresponding anion as expected, it is interesting to note that **4A** is less destabilized by the addition of a single electron than **4B**.

D. Anionic Water Hexamers, $(H_2O)_6^-$. As with the tetrameric structures, two types of systems were investigated: a highly symmetric hexamer (**6A**$^-$) possessing a 3-fold axis of symmetry and a cavity between two planes of hydrogen-bonded trimers and a less symmetric system (**6B**$^-$) which has a structure similar to a prism but is distorted at one end (Figure 6). Once again, the highly symmetric structure, **6A**$^-$, which possesses several NHB hydrogen atoms all directed toward the center of the cavity, exhibits a NNA. However, the hexameric cluster exhibits two key differences compared to the tetrameric case: (i) the NNA is now located in the center of the cavity formed by the water molecules, and (ii) the population of the NNA basin is much more significant, accommodating 0.23 e$^-$ (spin population of 0.23), contributing 21.5 kJ/mol to the overall energy of the system (Table 2) and a larger pseudo-atomic volume of 93.3 au. The spin populations for both **6A**$^-$ and **6B**$^-$ correlate well with the integration data and are graphically illustrated in the spin density plots (Figure 6). The excess electron in **6A**$^-$ is largely contained within the cavity, corresponding to the historical notion of the hydrated electron. On the other hand, **6B**$^-$ exhibits no such NNA, and upon investigation of the spin density plot (Figure 6), it is clear that this system largely accommodates the excess electron on a single water molecule on the surface of the cluster (with 0.23 and 0.28 e$^-$ on the H atoms involved and 0.30 e$^-$ on the oxygen; Table 2), similar to the distribution observed in the **2B**$^-$ system.

Subsequently, both structures were optimized as neutral species, resulting in geometrically similar structures compared to the anionic species. In particular, **6A** maintained the same arrangement of the water molecules as **6A**$^-$; however, the two planes are now closer together, and the NHB hydrogen atoms are bent away from the center of the cluster (Figure 6). Furthermore, the relative energies of these two species reveal that **6A**$^-$, the anion, is marginally more stable than **6A**, the neutral, by 7.4 kJ/mol. Even though the energy difference itself is negligible, the fact remains that this is the only system in which the anion and the corresponding neutral cluster are nearly equal in energy. Indeed, in most of the systems, the neutral cluster is more stable by approximately 50 kJ/mol or more. Although **6B**$^-$ is more stable than **6A**$^-$ by 34.9 kJ/mol, it is interesting to note that the addition of an electron to **6A** actually has a slight

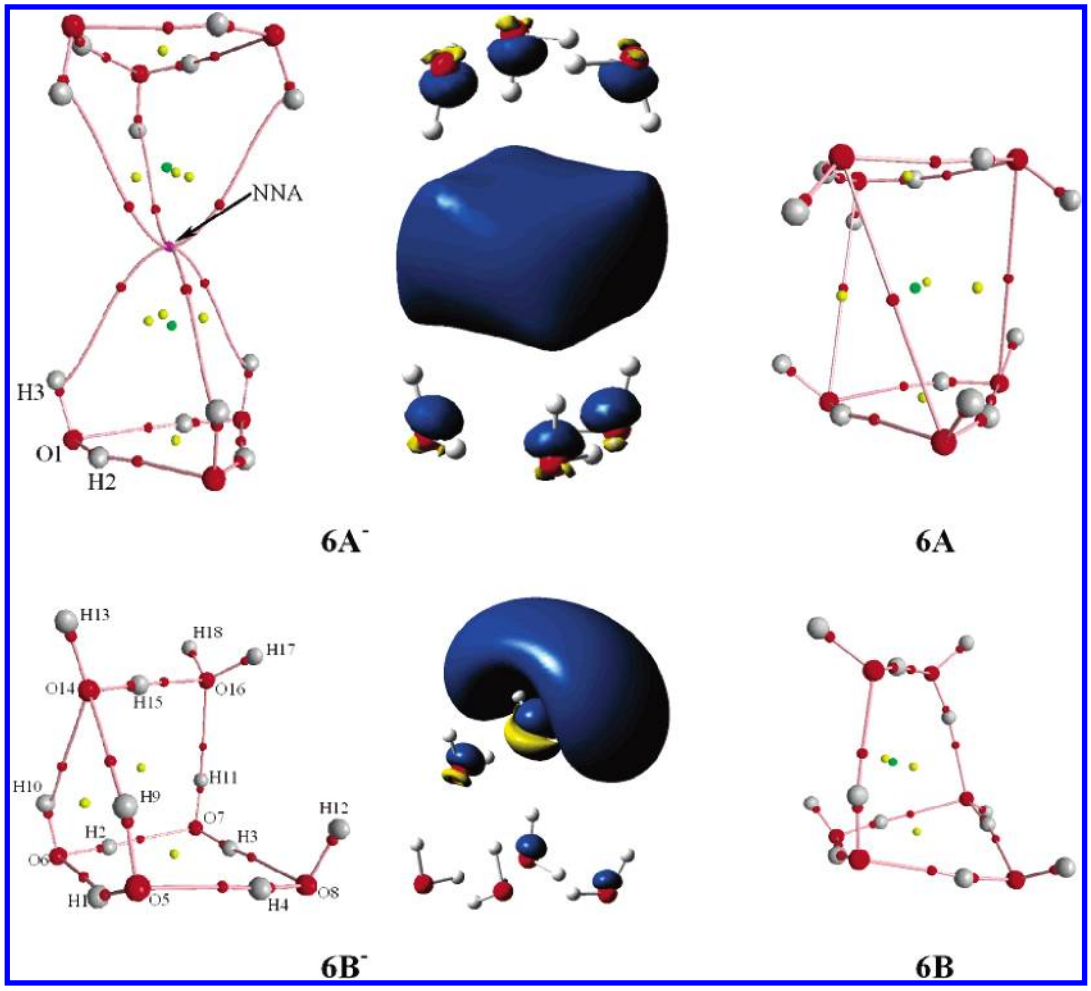

Figure 6. Molecular graphs of **6A**$^-$ and **6B**$^-$ with the 0.001 au spin density plots shown adjacent to each structure as well as the optimized structures of the neutral clusters **6A** and **6B**. Note the appearance of the NNA in the **6A**$^-$ system found in the center of the cavity formed between the two trimers.

stabilizing effect (or at least a negligible effect) while **6B** experiences a marked destabilization of 22.6 kJ/mol.

E. Anionic Water Octamers, $(H_2O)_8^-$. The final systems investigated were two anionic water octamers, constructed by placing two tetrameric planes on top of one another. The more symmetric of the two systems, **8A**$^-$, consists of two hydrogen-bonded planes of tetramers like **4A**$^-$ stacked so that the NHB hydrogen atoms are directed toward one another and the center of the cavity. However, the two stacked planes are not mirror images; one plane is rotated 45° relative to the other (Figure 7), maintaining the 4-fold axis of symmetry. The second system, **8B**$^-$, consists of two stacked tetramers like **4B** (neutral arrangement), forming a cube such that four of the water molecules have NHB hydrogen atoms directed away from the center of the cube while the other four water molecules form two hydrogen bonds each, giving the entire system a 2-fold axis of symmetry (Figure 7).

The more symmetric of the two systems, **8A**$^-$, exhibits a NNA at the center of the cavity, as may be expected on the basis of the hexameric results and the similarity between the two systems. The integration data reveal that this NNA possesses a significant portion of the excess electron, 0.22 e$^-$ (spin population of 0.21), contributes 17.9 kJ/mol to the overall energy of the system, and occupies a pseudo-atomic volume of 89.0 au. The remainder of the excess electron is largely accommodated on the NHB hydrogen atoms and the O atoms. Conversely, the **8B**$^-$ system exhibits no such NNA and tends to accommodate the excess electron on the O atoms and the NHB hydrogen atoms as per the other systems (see Table 2 for the exact charge distribution and spin populations). The different distributions are graphically illustrated in the spin density plots (Figure 7).

Upon optimization of the systems as neutral species, it was noted that the final neutral structure was the same for both cases, **8B** (Figure 7), which is very similar to **8B**$^-$ with some minor changes in bond lengths and angles. Comparing the relative energies of all eight-membered species, **8B** is more stable than either anion by more that 60 kJ/mol (Table 1). Moreover, **8B**$^-$ is merely 12.5 kJ/mol more stable than **8A**$^-$; one would expect **8B**$^-$ to be significantly more stable since it closely resembles the preferred neutral geometry. This last observation illustrates that although the two different distributions of the hydrated electron are qualitatively very different, they are in fact very similar energetically.

IV. Conclusions

QTAIM has been used to probe the nature of the solvated electron in small water clusters, $(H_2O)_n^-$, for $n = 1-8$. The

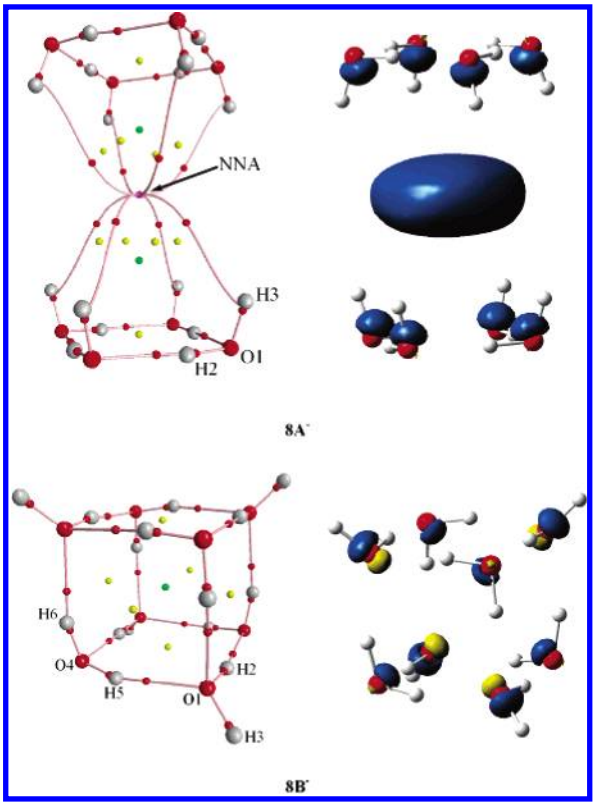

Figure 7. Molecular graphs of **8A**$^-$ and **8B**$^-$ with the 0.001 au spin density plots shown adjacent to each structure. Similar to the **6A**$^-$ system, a NNA appears in the center of the cavity formed between the two tetramers.

results indicate that the hydrated electron can take on one of several arrangements depending on the geometry of the cluster. Highly symmetric clusters, that can form a cavity between the water molecules and have several non-hydrogen-bonded H atoms directed toward this center (**2A**$^-$, **4A**$^-$, **6A**$^-$, and **8A**$^-$), favor the archetypical notion of the cavity-bound hydrated electron. Although clusters as small as four water molecules (**4A**$^-$) exhibit NNAs, only the larger clusters (**6A**$^-$ and **8A**$^-$) possess NNAs or pseudo-atoms with significant populations and energies (upward of 0.2 electrons and energy contributions in excess of 20 kJ/mol). On the other hand, the less symmetric clusters tend to distribute the excess electron on the surface of the cluster, either delocalized over the entire surface (**4B**$^-$ and **8B**$^-$) or localized on one specific water molecule (**2B**$^-$ and **6B**$^-$). A surface-bound solvated electron is observed in those cases where the NHB hydrogen atoms are directed away from the surface of the cluster while the cavity-bound model prevails when the NHB hydrogen atoms are oriented toward the center of the cavity. In general, the hydrated electron is accommodated on the non-hydrogen-bonded H atoms and the oxygen atoms, and it is the orientation of these non-hydrogen-bonded H atoms that dictates the distribution of the hydrated electron.

Acknowledgment. The authors gratefully acknowledge the Natural Sciences and Engineering Research Council of Canada, Dalhousie University, and the Killam Trusts for financial support. We thank Dr. Todd Keith for providing AIMALL97.

References

(1) Khan, A. *J. Chem. Phys.* **2006**, *125*, 024307.

(2) Sommerfeld, T.; Jordan, K. D. *J. Am. Chem. Soc.* **2006**, *128*, 5828.

(3) Coe, J. V.; Arnold, S. T.; Eaton, J. G.; Lee, G. H.; Bowen, K. H. *J. Chem. Phys.* **2006**, *125*, 014315.

(4) Baldacchino, G.; De Waele, V.; Monard, H.; Sorgues, S.; Gobert, F.; Larbre, J. P.; Vigneron, G.; Marignier, J. L.; Pommeret, S.; Mostafavi, M. *Chem. Phys. Lett.* **2006**, *424*, 77.

(5) De Waele, V.; Sorgues, S.; Pernot, P.; Marignier, J. L.; Monard, H.; Larbre, J. P.; Mostafavi, M. *Chem. Phys. Lett.* **2006**, *423*, 30.

(6) Neumann, S.; Eisfeld, W.; Sobolewski, A. L.; Domcke, W. *J. Phys. Chem. A* **2006**, 110, 5613.

(7) Lee, H. M.; Suh, S. B.; Tarakeshwar, P.; Kim, K. S. *J. Chem. Phys.* **2005**, *122*, 044309.

(8) Khan, A. *Chem. Phys. Lett.* **2005**, *401*, 85.

(9) Hammer, N. I.; Shin, J. W.; Headrick, J. M.; Diken, E. G.; Roscioli, J. R.; Weddle, G. H.; Johnson, M. A. *Science* **2004**, *306*, 675.

(10) Balaj, O. P.; Siu, C. K.; Balteanu, L.; Beyer, M. K.; Bondybey, V. E. *Int. J. Mass Spectrom.* **2004**, *238*, 65.

(11) Zhan, C. G.; Dixon, D. A. *J. Phys. Chem. B* **2003**, *107*, 4403.

(12) Beyer, M. K.; Fox, B. S.; Reinhard, B. M.; Bondybey, V. E. *J. Chem. Phys.* **2001**, *115*, 9288.

(13) Kulkarni, S. A.; Bartolotti, L. J.; Pathak, R. K. *J. Chem. Phys.* **2000**, *113*, 2697.

(14) Weigend, F.; Ahlrichs, R. *Phys. Chem. Chem. Phys.* **1999**, *1*, 4537.

(15) Smith, D. M. A.; Smets, J.; Adamowicz, L. *J. Chem. Phys.* **1999**, *110*, 3804.

(16) Chen, H. Y.; Sheu, W. S. *J. Chem. Phys.* **1999**, *110*, 9032.

(17) Tsurusawa, T.; Iwata, S. *Chem. Phys. Lett.* **1999**, *315*, 433.

(18) Ayotte, P.; Weddle, G. H.; Bailey, C. G.; Johnson, M. A.; Vila, F.; Jordan, K. D. *J. Chem. Phys.* **1999**, *110*, 6268.

(19) Kim, J.; Becker, I.; Cheshnovsky, O.; Johnson, M. A. *Chem. Phys. Lett.* **1998**, *297*, 90.

(20) Lee, S.; Kim, J.; Lee, S. J.; Kim, K. S. *Phys. Rev. Lett.* **1997**, *79*, 2038.

(21) Kim, K. S.; Park, I. J.; Lee, S.; Cho, K.; Lee, J. Y.; Kim, J.; Joannoupulos, J. D. *Phys. Rev. Lett.* **1996**, *76*, 956.

(22) Kimura, Y.; Alfano, J. C.; Walhout, P. K.; Barbara, P. F. *J. Phys. Chem.* **1994**, *98*, 3450.

(23) Coe, J. V.; Lee, G. H.; Eaton, J. G.; Arnold, S. T.; Sarkas, H. W.; Bowen, K. H.; Ludewigt, C.; Haberland, H.; Worsnop, D. R. *J. Chem. Phys.* **1990**, *92*, 3980.

(24) Barnett, R. N.; Landman, U.; Makov, G.; Nitzan, A. *J. Chem. Phys.* **1990**, *93*, 6226.

(25) Hameka, H. F.; Robinson, G. W.; Marsden, C. J. *J. Phys. Chem.* **1987**, *91*, 3150.

(26) Wallqvist, A.; Thirumalai, D.; Berne, B. J. *J. Chem. Phys.* **1986**, *85*, 1583.

(27) Haberland, H.; Schindler, H. G.; Worsnop, D. R. *Ber. Bunsen-Ges.* **1984**, *88*, 270.

(28) Haberland, H.; Ludewigt, C.; Schindler, H. G.; Worsnop, D. R. *J. Chem. Phys.* **1984**, *81*, 3742.

(29) Haberland, H.; Langosch, H.; Schindler, H. G.; Worsnop, D. R. *J. Phys. Chem.* **1984**, *88*, 3903.

(30) Armbruster, M.; Haberland, H.; Schindler, H. G. *Phys. Rev. Lett.* **1981**, *47*, 323.

(31) Copeland, D. A. *J. Chem. Phys.* **1970**, *53*, 1189.

(32) Stemmler, K.; von Gunten, U. *Atmos. Environ.* **2000**, *34*, 4241.

(33) Buxton, G. V.; Greenstock, C. L.; Helman, W. P.; Ross, A. B. *J. Phys. Chem. Ref. Data* **1988**, *17*, 513.

(34) Chameides, W. L. *Science* **1998**, *281*, 1152.

(35) Beal, M. F. *Trends Neurosci.* **2000**, *23*, 298.

(36) Weyl, W. *Ann. Phys. (Weinheim, Ger.)* **1864**, *121*, 601.

(37) Kraus, C. A. *J. Am. Chem. Soc.* **1908**, *30*, 1323.

(38) Hart, E. J.; Boag, J. W. *J. Am. Chem. Soc.* **1962**, *84*, 4090.

(39) Boag, J. W.; Hart, E. J. *Nature* **1963**, *197*, 45.

(40) Keene, J. P. *Nature* **1963**, *197*, 47.

(41) Schindewolf, U. *Angew. Chem., Int. Ed. Engl.* **1968**, *7*, 190.

(42) Migus, A.; Gauduel, Y.; Martin, J. L.; Antonetti, A. *Phys. Rev. Lett.* **1987**, *58*, 1559.

(43) Jortner, J.; Ottolenghi, M.; Stein, G. *J. Phys. Chem.* **1964**, *68*, 247.

(44) Walker, D. C. *Can. J. Chem.* **1966**, *44*, 2226.

(45) Knapp, M.; Echt, O.; Kreisle, D.; Recknagel, E. *J. Chem. Phys.* **1986**, *85*, 636.

(46) Knapp, M.; Echt, O.; Kreisle, D.; Recknagel, E. *J. Phys. Chem.* **1987**, *91*, 2601.

(47) Balaj, O. P.; Balteanu, I.; Fox-Beyer, B. S.; Beyer, M. K.; Bondybey, V. E. *Angew. Chem., Int. Ed.* **2003**, *42*, 5516.

(48) Barnett, R. N.; Landman, U.; Cleveland, C. L.; Jortner, J. *J. Chem. Phys.* **1988**, *88*, 4429.

(49) Feng, D. F.; Kevan, L. *Chem. Rev.* **1980**, *80*, 1.

(50) Kevan, L. *Acc. Chem. Res.* **1981**, *14*, 138.

(51) Fueki, K. *J. Am. Chem. Soc.* **1973**, *95*, 1398.

(52) Gaathon, A.; Jortner, J. In *Electrons in Fluids*; Jortner, J., Kestner, N. R., Eds.; Springer: Berlin, 1973; p 429.

(53) Schnitker, J.; Rossky, P. J. *J. Chem. Phys.* **1987**, *86*, 3471.

(54) Rossky, P. J.; Schnitker, J. *J. Phys. Chem.* **1988**, *92*, 4277.

(55) Khan, A. *J. Chem. Phys.* **2003**, *118*, 1684.

(56) Turi, L.; Sheu, W. S.; Rossky, P. J. *Science* **2005**, *309*, 914.

(57) Tauber, M. J.; Mathies, R. A. *J. Am. Chem. Soc.* **2003**, *125*, 1394.

(58) Kim, J.; Lee, J. Y.; Oh, K. S.; Park, J. M.; Lee, S.; Kim, K. S. *Phys. Rev. A* **1999**, *59*, R930.

(59) Kim, J.; Suh, S. B.; Kim, K. S. *J. Chem. Phys.* **1999**, *111*, 10077.

(60) Suh, S. B.; Lee, H. M.; Kim, J.; Lee, J. Y.; Kim, K. S. *J. Chem. Phys.* **2000**, *113*, 5273.

(61) Novakovskaya, Y. V.; Stepanov, N. F. *J. Phys. Chem. A* **1999**, *103*, 10975.

(62) Clary, D. C.; Benoit, D. M. *J. Chem. Phys.* **1999**, *111*, 10559.

(63) Rao, B. K.; Kestner, N. R. *J. Chem. Phys.* **1984**, *80*, 1587.

(64) Kestner, N. R.; Jortner, J. *J. Phys. Chem.* **1984**, *88*, 3818.

(65) Landman, U.; Barnett, R. N.; Cleveland, C. L.; Scharf, D.; Jortner, J. *J. Phys. Chem.* **1987**, *91*, 4890.

(66) Barnett, R. N.; Landman, U.; Cleveland, C. L.; Jortner, J. *J. Chem. Phys.* **1988**, *88*, 4421.

(67) Barnett, R. N.; Landman, U. *Phys. Rev. Lett.* **1993**, *70*, 1775.

(68) Jortner, J. *J. Chem. Phys.* **1959**, *30*, 839.

(69) Bader, R. F. W. *Atoms in Molecules: A Quantum Theory*; Oxford University Press: Oxford, U. K., 1990.

(70) Bader, R. F. W.; Nguyen Dang, T. T. *Adv. Quantum Chem.* **1981**, *14*, 63.

(71) Bader, R. F. W. *Chem. Rev.* **1991**, *91*, 893.

(72) Popelier, P. L. A. *Atoms in Molecules: An Introduction*; Prentice Hall: London, 2000.

(73) Matta, C. F.; Boyd, R. J. *The Quantum Theory of Atoms in Molecules: From Solid State to DNA and Drug Design*; Wiley-VCH: Weinheim, Germany, 2007.

(74) Bader, R. F. W. *J. Phys. Chem. A* **1998**, 102, 7314.

(75) Keith, T. A.; Bader, R. F. W.; Aray, Y. *Int. J. Quantum Chem.* **1996**, *57*, 183.

(76) Bader, R. F. W.; Matta, C. F. *Organometallics* **2004**, *23*, 6253.

(77) Bader, R. F. W. *Phys. Rev. B* **1994**, *49*, 13348.

(78) Schwinger, J. *Phys. Rev.* **1951**, *82*, 914.

(79) Bader, R. F. W.; Popelier, P. L. A. *Int. J. Quantum Chem.* **1993**, *45*, 189.

(80) Matta, C. F.; Bader, R. F. W. *J. Phys. Chem. A* **2006**, 110, 6365.

(81) Collard, K.; Hall, G. G. *Int. J. Quantum Chem.* **1977**, *12*, 623.

(82) Gatti, C.; Fantucci, P.; Pacchioni, G. *Theor. Chim. Acta* **1987**, 72, 433.

(83) Cao, W. L.; Gatti, C.; Macdougall, P. J.; Bader, R. F. W. *Chem. Phys. Lett.* **1987**, *141*, 380.

(84) Mei, C. J.; Edgecombe, K. E.; Smith, V. H.; Heilingbrunner, A. *Int. J. Quantum Chem.* **1993**, *48*, 287.

(85) Iversen, B. B.; Larsen, F. K.; Souhassou, M.; Takata, M. *Acta Crystallogr., Sect. B* **1995**, 51, 580.

(86) Iversen, B. B.; Larsen, F. K. In *Collected Abstracts*, XVII Congress, International Union of Crystallography, Seattle, Washington, August 8−17, 1996; International Union of Crystallography: Seattle, Washington, 1996.

(87) Frisch, M. J.; Trucks, G. W.; Schlegel, H. B.; Scuseria, G. E.; Robb, M. A.; Cheeseman, J. R.; Montgomery, J. J. A.; Vreven, T.; Kudin, K. N.; Burant, J. C.; Millam, J. M.; Iyengar, S. S.; Tomasi, J.; Barone, V.; Mennucci, B.; Cossi, M.; Scalmani, G.; Rega, N.; Petersson, G. A.; Nakatsuji, H.; Hada, M.; Ehara, M.; Toyota, K.; Fukuda, R.; Hasegawa, J.; Ishida, M.; Nakajima, T.; Honda, Y.; Kitao, O.; Nakai, H.; Klene, M.; Li, X.; Knox, J. E.; Hratchian, H. P.; Cross, J. B.; Bakken, V.; Adamo, C.; Jaramillo, J.; Gomperts, R.; Stratmann, R. E.; Yazyev, O.; Austin, A. J.; Cammi, R.; Pomelli, C.; Ochterski, J. W.; Ayala, P. Y.; Morokuma, K.; Voth, G. A.; Salvador, P.; Dannenberg, J. J.; Zakrzewski, V. G.; Dapprich, S.; Daniels, A. D.; Strain, M. C.; Farkas, O.; Malick, D. K.; Rabuck, A. D.; Raghavachari, K.;

Foresman, J. B.; Ortiz, J. V.; Cui, Q.; Baboul, A. G.; Clifford, S.; Cioslowski, J.; Stefanov, B. B.; Liu, G.; Liashenko, A.; Piskorz, P.; Komaromi, I.; Martin, R. L.; Fox, D. J.; Keith, T.; Al-Laham, M. A.; Peng, C. Y.; Nanayakkara, A.; Challacombe, M.; Gill, P. M. W.; Johnson, B.; Chen, W.; Wong, M. W.; Gonzalez, C.; Pople, J. A. *Gaussian 03*, Revision B.05; Gaussian, Inc.: Wallingford, CT, 2004.

(88) Biegler-Konig, F.; Schonbohm, J.; Bayles, D. *J. Comput. Chem.* **2001**, 22, 545.

(89) Biegler-Konig, F. W.; Bader, R. F. W.; Tang, T. *J. Comput. Chem.* **1982**, *3*, 317.

(90) Keith, T. A. *AIMALL97 for DOS/Windows*, private communication, 1997.

(91) Dennington, R., II; Keith, T.; Millam, J.; Eppinnett, K.; Hovell, W. L.; Gilliland, R. *GaussView*, Version 3.09; Semichem, Inc.: Shawnee Mission, KS, 2003.

CT600334W